Magnetic properties of the overdoped superconductor $La_{2-x}Sr_xCuO_4$ with and without Zn impurities

S. Wakimoto,[1,2,*] R. J. Birgeneau,[1,3] A. Kagedan,[1] Hyunkyung Kim,[1] I. Swainson,[4] K. Yamada,[5] and H. Zhang[1]
[1]*Department of Physics, University of Toronto, Toronto, Ontario, Canada M5S 1A7*
[2]*Advanced Science Research Center, Japan Atomic Energy Research Institute, Tokai, Ibaraki 319-1195, Japan*
[3]*Department of Physics, University of California, Berkeley, Berkeley, California 94720-7300, USA*
[4]*Neutron Program for Materials Research, National Research Council of Canada, Chalk River, Ontario, Canada K0J 1J0*
[5]*Institute of Material Research, Tohoku University, Katahira, Sendai 980-8577, Japan*
(Received 21 March 2005; published 25 August 2005)

The magnetic properties of the Zn-substituted overdoped high-T_c superconductor $La_{2-x}Sr_xCu_{1-y}Zn_yO_4$ have been studied by magnetization measurements and neutron scattering. Magnetization measurements reveal that for Zn-free samples with $x \geqslant 0.22$ a Curie term is induced in the temperature dependence of the magnetic susceptibility implying the existence of local paramagnetic moments. The induced Curie constant corresponds to a moment of 0.5 μ_B per additional Sr^{2+} ion that exceeds $x=0.22$. Zn substitution in the overdoped $La_{2-x}Sr_xCuO_4$ also induces a Curie term that corresponds to 1.2 μ_B per Zn^{2+} ion, simultaneously suppressing T_c. The relationship between T_c and the magnitude of the Curie term for Zn-free $La_{2-x}Sr_xCuO_4$ with $x \geqslant 0.22$ and for Zn-substituted $La_{2-x}Sr_xCuO_4$ with $x=0.22$ are closely similar. This signifies a general competitive relationship between the superconductivity and the induced paramagnetic moment. Neutron scattering measurements show that Zn substitution in overdoped $La_{2-x}Sr_xCuO_4$ anomalously enhances the inelastic magnetic scattering spectra around the (π, π) position, peaking at $\omega \sim 7$ meV. These facts are discussed on the basis of a "swiss-cheese" model of Zn-substituted systems as well as a microscopic phase separation scenario in the overdoped region indicated by muon-spin-relaxation measurements.

DOI: 10.1103/PhysRevB.72.064521 PACS number(s): 74.72.Dn, 75.40.Gb, 75.40.Cx, 61.12.Ex

I. INTRODUCTION

Neutron scattering studies of the magnetic response in the hole-doped high-T_c cuprates up to the optimally doped region have revealed rich and complex behavior of the static and dynamic spin correlations. For the $La_{2-x}Sr_xCuO_4$ (LSCO) system, an incommensurate modulation at low energies has been found around the antiferromagnetic (AF) wave vector[1–3] with the incommensurability, defined as the inverse of the modulation period, proportional to the hole concentration.[4] Moreover, at the lower critical hole concentration of superconductivity, with increasing doping the modulation direction changes from the diagonal Cu-Cu direction in the insulator region to the parallel Cu-O-Cu direction in the superconducting (SC) region.[5–8] Such incommensurate magnetic features have been discussed on the basis of a microscopically inhomogeneous electronic state of which the most commonly discussed example is charge stripes.[9–12]

For the $YBa_2Cu_3O_{6+z}$ (YBCO) system, although the same type of low energy incommensurate magnetic response has been confirmed,[13–17] the most prominent feature is a resonance peak that originates from a strong magnetic excitation at intermediate energies ($\sim$40 meV) at the commensurate AF vector. It has been hypothesized that the resonance is directly related to the superconductivity.[16–19] The resonance feature has been observed for other hole doped high-T_c cuprates as well,[20,21] although until recently attempts to establish the universality of the resonance peak have been unsuccessful. However, recent high energy measurements on YBCO,[22–24] $La_{2-x}Br_xCuO_4$,[25] and LSCO[26] have indeed suggested a universal magnetic response; specifically, in each material the low energy incommensurate excitation disperses inwards with increasing energy and meets at the commensurate AF vector; the excitation then again disperses outwards in an approximately symmetric fashion in the high energy region.

These facts suggest that subtly different spectral weight distributions in the universal dispersion discussed above give rise to the apparently different magnetic responses in each compound. In the case of the LSCO system, there is a relatively large spectral weight in the low energy incommensurate excitations. The LSCO system provides the fortunate possibility of systematically studying the behavior over an extremely wide range of hole concentrations from the underdoped to the overdoped region. To date, however, the magnetic properties in the overdoped region are not well understood. Recent neutron scattering experiments[27] have revealed a surprising feature in the magnetism in overdoped LSCO. These measurements show that the integrated dynamic spin susceptibility $\chi''(\omega)$ has a maximum at $\omega \sim 6$ meV and this maximum $\chi''(\omega)$ decreases linearly with T_c for samples with $x \geqslant 0.25$. Finally the low energy magnetic response disappears coincident with the disappearance of bulk superconductivity at $x=0.30$. Therefore the low-energy incommensurate excitations are intimately connected with the superconductivity.

In the present paper we report a study of the magnetism in overdoped LSCO with and without Zn impurities. Neutron scattering and magnetic susceptibility measurements elucidate the dependence of the superconductivity on certain features of the low energy magnetism in the overdoped region. Magnetic susceptibility measurements of LSCO with $0.18 \leqslant x \leqslant 0.28$ reveal that the temperature dependence of the

susceptibility $\chi(T)$ for $x \leqslant 0.22$ falls on the universal curve originally reported by Johnston,[28] while $\chi(T)$ for $x \geqslant 0.22$ exhibits in addition Curie paramagnetism; these results are qualitatively consistent with those of Oda *et al.*[29–31] By comparing results in overdoped LSCO with and without Zn impurities, it is found that both hole-overdoping and Zn substitution induce Curie paramagnetism as well as a decrease in T_c in the same manner, although Zn substitution has a stronger effect. This implies a general competitive relationship between the superconductivity and the $\mathbf{q}=0$ Curie paramagnetism. Neutron scattering experiments for Zn-substituted LSCO with $x=0.20$ and 0.25 exhibit an anomalous enhancement of the incommensurate inelastic magnetic scattering around the $(\pi\ \pi)$ position. Zn-substituted samples exhibit the same incommensurability and coherence length, while the enhancement in the $x=0.25$ sample is smaller than that in $x=0.20$. These facts are apparently consistent with a "swiss-cheese" model of Zn-impurity effects[32] and a microscopic phase separation model of the overdoped cuprates hypothesized from muon-spin-relaxation (μSR) measurements.[33]

The organization of this paper is as follows. In Sec. II, the experimental details are presented. Results of the magnetic susceptibility measurements of $La_{2-x}Sr_xCu_{1-y}Zn_yO_4$ (LSCZO) together with an empirical scaling relation of the high temperature susceptibility are introduced in Sec. III. Neutron scattering results of hole-overdoped LSCZO are reported in Sec. IV. Finally, the results are discussed on the basis of the swiss-cheese model and the phase separation model in Sec. V and then summarized in Sec. VI.

II. EXPERIMENTAL DETAILS

For the magnetization measurements, a series of ceramic samples of LSCZO were synthesized by the conventional solid state reaction method. The appropriate stoichiometric quantities of the starting materials, La_2O_3, $SrCO_3$, CuO, and ZnO were ground and baked in air for 12 h at 900 °C followed by an additional grinding process. The reacted powder was then pelletized under hydrostatic pressure and sintered in air at 900 °C for 10 h and at 1150 °C for an additional 10 h. Finally, the pelletized samples were annealed in flowing oxygen gas at 850 °C for 12 h to restore any oxygen deficiencies in their composition.

The magnetic susceptibility measurements were carried out using a Quantum Design physical property measurement system (PPMS). The samples were mounted at the end of a plastic straw with a small amount of Kapton tape. The sample chamber was purged 20 times at room temperature before each measurement in order to minimize any air presence in the measurement environment. The SC shielding effect was measured with a field of 10 Oe after cooling under zero field to determine the SC transition temperature T_c. The high temperature magnetic susceptibility was measured with a field of 5 T over a temperature range of 20–350 K after cooling under zero field.

For the neutron scattering measurements, single crystals of LSCZO were grown by the traveling solvent floating zone method.[34,35] Feed rods were prepared in the same manner as the ceramic samples mentioned above aside from the addition of excess CuO of 2 to 3 mol % to compensate for the evaporation of CuO during the high temperature growth. The grown crystals were cut into the proper size for neutron scattering and then were annealed in flowing oxygen for 100 h at 900 °C. Each prepared crystal had a typical size of 7 mm in diameter and 3.5 cm in length.

Inelastic neutron scattering experiments were performed using the C5 spectrometer at Chalk River Laboratory for all samples except the Zn-free $x=0.20$ sample, and the TAS1 spectrometer at the Japan Atomic Energy Research Institute for the Zn-free $x=0.20$ sample. A fixed final energy (E_f) of 14.5 meV ($\lambda=2.37$ Å) and the collimation sequence of $33'$-$48'$-$51'$-$120'$ were used for the former spectrometer while for the latter the configuration was $E_f=14.7$ meV and $40'$-$80'$-$80'$-open. Pyrolytic graphite (PG) crystals were used as a monochromator and an analyzer. A PG filter was placed between the sample and the analyzer to eliminate higher order neutrons with wavelengths $\lambda/2$ and $\lambda/3$. For each concentration, two single crystals were coaligned on an Al sample holder with the a and b axes in the scattering plane, and then mounted in a closed cycle He refrigerator.

All samples except the $x=0.20$ sample are tetragonal down to the lowest temperature with typical lattice constants of $a=b=3.73$ Å, corresponding to reciprocal lattice units of $a^*=b^*=1.68$ Å^{-1} in tetragonal notation with space group $I4/mmm$. The $x=0.20$ sample exhibits a structural phase transition from the high-temperature tetragonal to the low-temperature orthorhombic phase at $\sim$70 K, in good agreement with previous work.[36] Throughout this paper we use tetragonal notation to express the indices.

III. MAGNETIC SUSCEPTIBILITY

A. Scaling behavior

Before we present the results of our magnetic susceptibility measurements, we introduce the previously determined empirical scaling relation. Johnston[28] has systematically measured the temperature dependence of the magnetic susceptibility $\chi(x,T)$ of LSCO for $0 \leqslant x \leqslant 0.2$ and represented the data by the formula

$$\chi(x,T) = \chi_0(x) + \chi^{2D}(x,T), \tag{1}$$

where χ_0 is the temperature independent uniform susceptibility and $\chi^{2D}(x,T)$ is the temperature dependent in-plane susceptibility. Johnston has reported that if one assumes the proper value for $\chi_0(x)$, then χ^{2D} follows the simple scaling relation

$$F(T/T_{max}(x)) = \frac{\chi^{2D}(T,x)}{\chi^{2D}_{max}(T_{max},x)}, \tag{2}$$

where F is a universal function and χ^{2D}_{max} is the maximum value of χ^{2D} at $T=T_{max}$. This scaling relation has been reexamined in detail by Oda *et al.*[29] for a wide concentration range of LSCO and LBCO. They observed that beyond the hole concentration of $x=0.18$ in LSCO, T_{max} saturates and $\chi(x,T)$ begins to deviate from the universal scaling function. Furthermore, this deviation takes the form of a Curie paramagnetic term. Thus, in the overdoped region, the susceptibility can be expressed as

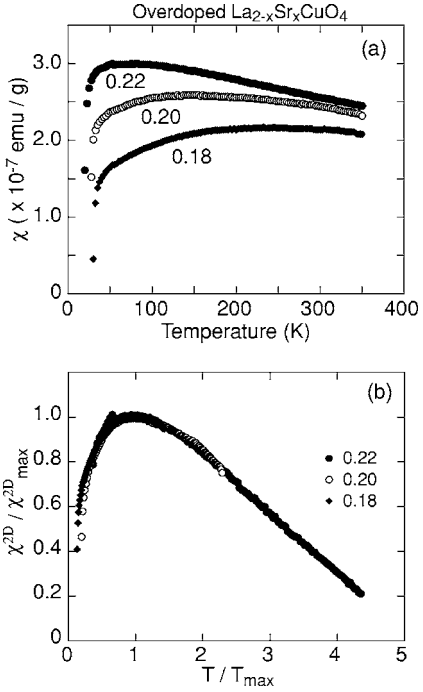

FIG. 1. (a) Temperature dependence of the magnetic susceptibility for $x=0.18$, 0.20, and 0.22. The extreme drop off in $\chi(T,x)$ at very low T is due to the SC transition. (b) Universal scaling function, $F(T/T_{max})=\chi^{2D}/\chi^{2D}_{max}$, for the noted hole concentrations.

$$\chi(x,T) = \chi_0(x) + \chi^{2D}(x,T) + \frac{C}{T}, \tag{3}$$

where C is the Curie constant.

We present first the scaling relation in the current polycrystalline samples that were annealed systematically in the same manner. The temperature dependences of the magnetic susceptibility, $\chi(x,T)$, for hole concentrations of $x=0.18$, 0.20, and 0.22 are shown in Fig 1(a). The data display a clear shift in T_{max} to lower T with increasing hole concentration, qualitatively consistent with previous results.[28–30] These $\chi(x,T)$ curves can be scaled excellently by Eq. (2) as shown in Fig. 1(b). The values of T_{max}, χ_{max}, and χ_0 used to scale the data are summarized in Table I, where χ_{max} is defined as $\chi_{max}=\chi^{2D}_{max}+\chi_0$. The increase of χ_0 with increasing hole concentration x is probably due to the increase of the Pauli susceptibility, again qualitatively consistent with previous results.

B. Curie paramagnetism

As the doping is increased beyond $x=0.22$, we have observed that a Curie paramagnetic term appears in the $\chi(x,T)$ curve. Figure 2(a) shows the $\chi(x,T)$ curves for $x=0.22$ and 0.24, the latter of which cannot be scaled by Eq. (2). Instead, the differential $\chi(x=0.24)-\chi(x=0.22)$ can be fitted excellently by the Curie term $C/T+\Delta\chi_0$ with Curie constant $C=1.25\times10^{-6}$ emu K/g as shown in Fig. 2(b). The constant term $\Delta\chi_0$ is included to account for a possible change of the "background" susceptibility due to variations in both χ_0 and the measurement environment. The excellent agreement between the data and the fit indicates that for $x>0.22$ a simple Curie paramagnetic component appears in addition to the universally scaled χ^{2D}. Although there is a difference in the onset concentration where the Curie term starts to appear, possibly due to a difference in the postannealing condition, the present results are qualitatively consistent with those of Oda *et al.*[29] Thus the overdoping of charge carriers in the LSCO system induces Curie paramagnetism and reduces T_c.

TABLE I. T_{max}, χ_{max}, and χ_0 for hole concentrations $x=0.18$, 0.20, and 0.22. χ_{max} is defined as $\chi_{max}=\chi^{2D}_{max}+\chi_0$.

x	T_{max} (K)	χ_{max} (10^{-7} emu/g)	χ_0 (10^{-7} emu/g)
0.18	245.0	2.167	0.5
0.20	152.7	2.592	1.5
0.22	80.5	2.99	2.3

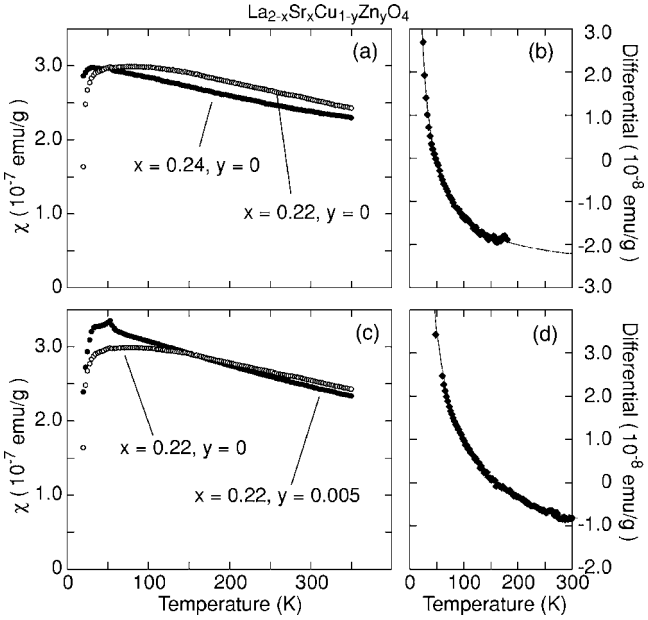

FIG. 2. (a) Temperature dependence of the magnetic susceptibilities of Zn-free samples with $x=0.22$ and 0.24. (b) Differential plot of $\chi(x=0.24)-\chi(x=0.22)$. (c) Magnetic susceptibilities of the Zn-free $x=0.22$ sample and a Zn-doped sample with $x=0.22$ and $y=0.005$. A sharp small peak at $\sim$50 K in the data for $(x,y)=(0.22,0.005)$ is due to the condensation of a small amount of oxygen in the sample chamber. (d) Differential plot of $\chi(x=0.22,y=0)-\chi(x=0.22,y=0.005)$. For (b) and (d), the lines are the results of fits to the Curie term C/T.

Similar to these effects, it is well-known that the substitution of small amounts of Cu^{2+} ions with nonmagnetic ions, such as Zn^{2+}, induces Curie paramagnetism and eliminates superconductivity. To compare these effects, one by Sr overdoping and the other by Zn substitution, we studied the magnetic susceptibility of $La_{2-x}Sr_xCu_{1-y}Zn_yO_4$. Figure 3 highlights the correlation between the dopant concentration and the observed decrease in T_c which implies the extinction of superconductivity. Note that the horizontal axis shows the total amount of dopant $x+y$. Closed circles, representing the data for the Zn-free ($y=0$) samples, indicate a gradual decrease of T_c with increasing x. T_c for the Zn-free single crystals referred from Ref. 27 are also shown by diamonds, dem-

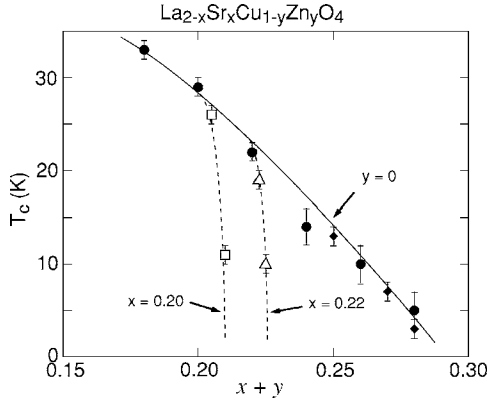

FIG. 3. Decrease in T_c due to the combination of increased hole concentration and Zn doping in the overdoped regime. Note that the horizontal axis indicates the summation of both dopant concentrations $x+y$ of $La_{2-x}Sr_xCu_{1-y}Zn_yO_4$. The circles represent data for the Zn-free samples. The diamonds represent T_c for Zn-free single crystals referred from Ref. 27. The squares and triangles represent data for the Zn-doped $x=0.20$ and 0.22 samples, respectively. The Zn amounts are $y=0.005$ and 0.01 in order of decreasing T_c for $x=0.20$, and $y=0.0025$ and 0.05 for $x=0.22$.

onstrating excellent agreement with our results on the present powder samples. In contrast, the data for the Zn-substituted samples with fixed Sr concentrations $x=0.20$ and 0.22 indicated by squares and triangles, respectively, show a drastic decrease of T_c with increasing y.

As expected, Zn substitution in the samples in the overdoped regime also induces Curie paramagnetism. Figure 2(c) shows $\chi(T)$ curves for two $x=0.22$ samples with $y=0$ and 0.005. The latter sample shows a small sharp peak at $\sim$50 K which arises from the condensation of oxygen in the measurement environment as a result of inadvertently not achieving a proper vacuum in the measurement chamber for those particular data. The differential of $\chi(x=0.22, y=0.005)-\chi(x=0.22, y=0)$ excluding the temperature range where the oxygen peak appears is shown in Fig. 2(d). Again the differential can be fitted excellently by a simple Curie term with $C=2.59\times10^{-6}$ emu K/g. Thus Zn substitution induces effects on the magnetism and superconductivity which are exactly analogous to those caused by Sr doping for $x\geqslant0.22$.

The present data for the magnetic susceptibility for $La_{2-x}Sr_xCu_{1-y}Zn_yO_4$ are summarized in Fig. 4. These data evince a clear correlation between a decrease of T_c and an increase of the Curie constant. From the results for the Zn-doped samples with fixed Sr concentration at $x=0.20$ shown by squares together with the datum point for the Zn-free sample indicated by an open circle, we conclude that increasing the Zn ion concentration reduces T_c and increases the Curie constant. The solid line is the result of a fit of these three datum points represented by open symbols to a linear function $T_c=\alpha\times C+T_c(x=0.20, y=0)$ which gives $\alpha=-3.8(\pm0.3)\times10^6$ g/emu. Similarly, starting from a Zn-free $x=0.22$ sample, both further doping of Sr and Zn substitution reduce T_c as well as increase C in a similar manner as shown by the closed circles and triangles, respectively. These data

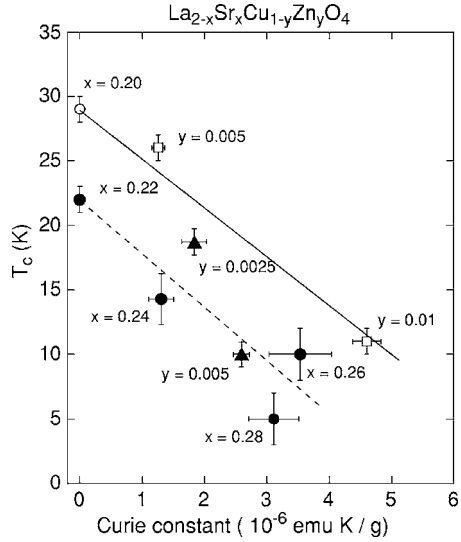

FIG. 4. T_c as a function of Curie constant for the $La_{2-x}Sr_xCu_{1-y}Zn_yO_4$ samples in the overdoped regime. Circles are data for the Zn-free samples. Squares and triangles indicate data for Zn-doped $x=0.20$ and 0.22 samples, respectively. The solid line is the result of a fit of the datum points for samples with $x=0.20$ shown by open symbols to a linear function $T_c=\alpha\times C+T_c(x=0.20, y=0)$, while the dashed line is the result of a fit of the rest of the datum points shown by closed symbols to a linear function $T_c=\alpha\times C+T_c(x=0.22, y=0)$.

may also be fit to a linear function $T_c=\alpha\times C+T_c(x=0.22, y=0)$. The best fit, shown by the dashed line, is given by $\alpha=-4.2(\pm0.6)\times10^6$ g/emu, which is the same as that for the Zn doped $x=0.20$ samples. Thus, very interestingly, the overdoping of Sr for $x\geqslant0.22$ and Zn substitution exhibit closely analogous effects, namely a decrease of T_c with increasing C, although the Zn substitution has a much stronger effect. This implies a general competitive relationship between the superconductivity and the Curie paramagnetism. Most importantly, it implies that in the overdoped regime for $x\geqslant0.22$ increasing the Sr concentration creates local moments which in turn destroy the superconductivity.

IV. DYNAMIC ANTIFERROMAGNETIC CORRELATIONS

Neutron scattering experiments have been performed to probe any differences in the antiferromagnetic (AF) correlations between Zn-free and Zn-substituted overdoped LSCO. The observed magnetic cross section can be written as

$$\frac{\partial^2\sigma}{\partial\Omega\partial\omega}=A\frac{1}{\hbar}p^2f^2(Q)e^{-2W}\frac{2\chi''(\mathbf{Q},\omega)}{\pi\mu_B^2}(n+1), \qquad (4)$$

where p is the magnetic scattering length 0.27×10^{-12} cm, $f(Q)$ is the magnetic form factor, e^{-2W} is the Debye-Waller factor, μ_B is the Bohr magneton, and $(n+1)$ is the thermal population factor. To compare the dynamic spin susceptibility $\chi''(\mathbf{Q},\omega)$ between Zn-free and Zn-substituted samples, the observed cross section has been normalized by the integrated phonon intensity

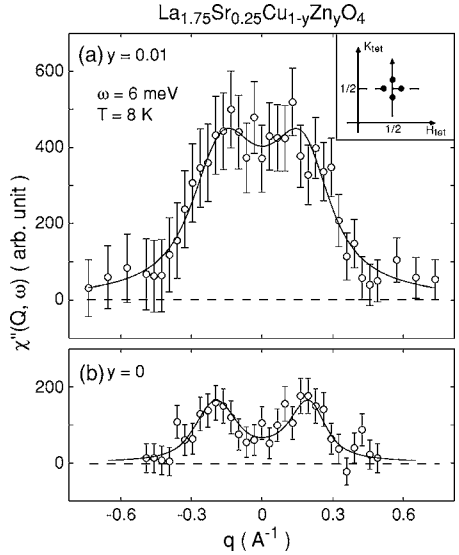

FIG. 5. Dynamic spin susceptibility $\chi''(\mathbf{Q},\omega)$ at $\mathbf{Q}=(1/2+q,1/2)$ and $\omega=6$ meV for (a) Zn-substituted ($y=0.01$) and (b) Zn-free LSCO with $x=0.25$. $\chi''(\mathbf{Q},\omega)$ is calculated by normalizing to the phonon intensity after a background subtraction. The solid lines are the results of fits to a resolution-convoluted two-dimensional Lorentzian function.

$$I = A\frac{1}{2\omega_p}\frac{|\mathbf{Q}|^2\cos\beta}{M}|F(Q)|^2(n+1), \tag{5}$$

where ω_p is the phonon frequency, β is the angle between $\mathbf{Q}$ and the phonon polarization vector, M is the molecular weight, and $|F(\mathbf{Q})|$ is the structure factor. Details of the normalization procedure are given in the Appendix including raw data of phonon and magnetic cross sections. The $\chi''(\mathbf{Q},\omega)$ so obtained has been fitted to a resolution-convoluted two-dimensional Lorentzian function to derive the incommensurability δ and the intrinsic peak width $\kappa(\omega)$:

$$\chi''(\mathbf{Q},\omega) \propto \sum_i \frac{1}{(\mathbf{Q}-\mathbf{Q}_i)^2+\kappa(\omega)^2}, \tag{6}$$

where the summation over i has been carried out for the four incommensurate peaks at $(1/2\pm\delta,1/2)$ and $(1/2,1/2\pm\delta)$.

Figure 5 shows $\chi''(\mathbf{Q},\omega)$ for the Zn-free and Zn-substituted $x=0.25$ samples at $\omega=6.2$ meV which is the energy at which the dynamic susceptibility of the Zn-free sample has a maximum. The scan was made along the trajectory $(1/2,1/2+q)$ as shown by the arrow in the inset. The data for $y=0$ in Fig. 5(b) are taken from Ref. 27. Clearly, there is an anomalous enhancement of $\chi''(\mathbf{Q},\omega)$ as a result of the Zn substitution. Furthermore, the Zn-substituted sample exhibits a somewhat flat-top shape profile possibly due to a smaller incommensurability and larger peak width. Identical effects are observed in the $x=0.20$ samples as shown in Fig. 6. However, accounting for the different scales of the vertical axes in Figs. 6 and 5, it is evident that the $x=0.20$ sample with $y=0.005$ has a larger enhancement of $\chi''(\mathbf{Q},\omega)$ than the $x=0.25$ sample with $y=0.01$.

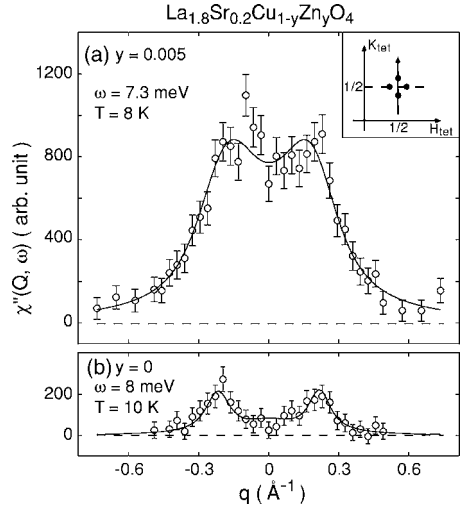

FIG. 6. Analogous plots to Fig. 5 of $\chi''(\mathbf{Q},\omega)$ for the (a) Zn-substituted ($x=0.005$) and (b) Zn-free LSCO with $x=0.20$. Note that the vertical axis scale is different from that of Fig. 5.

Before discussing the enhancement of $\chi''(\mathbf{Q},\omega)$ in detail, we first consider the changes in the incommensurability δ and intrinsic width $\kappa(\omega)$ evinced by fitting the data to the resolution-convoluted Eq. (6). The results of the fits are shown as the solid lines in Figs. 5 and 6, and the parameters δ and $\kappa(\omega)$ are summarized in Table II. Consistent with previous work,[4,37,38] the incommensurability δ for the Zn-free samples saturates at $\sim 1/8$. However, a small amount of Zn appears to reduce the incommensurability by $\sim 10\%$. The effect on $\kappa(\omega)$ is even more dramatic; the Zn-substituted samples show $\kappa(\omega)$ increased by factors of 2 and 3 in the $x=0.25$ and 0.20 samples, respectively. It is interesting to note that the values of $\kappa(\omega)$ for the Zn-substituted samples are almost identical, although the Zn-free samples exhibit a very different value for $\kappa(\omega)$ for the samples with $x=0.20$ and 0.25, respectively.

It is an open question why the incommensurability appears to decrease in the Zn-doped samples. We note that the peak profile for the sample with $x=0.25$ and $y=0.01$ in Fig. 5(a) can be alternatively reproduced approximately by a summation of a commensurate peak and the $\chi''(\mathbf{Q},\omega)$ of the Zn-free $x=0.25$, implying the possibility that Zn doping adds a commensurate feature; this is in place of the explanation given above that Zn-doping enhances the incommensurate magnetic correlations. Either interpretation, however, is consistent with the conclusions drawn in the later sections.

Next, we present the enhancement of the spin susceptibility. Figure 7 shows the ω-dependence of the q-integrated

TABLE II. Incommensurability δ in reciprocal lattice units (r.l.u.) and intrinsic width κ obtained by fitting the data to Eq. (6).

x	y	δ (r.l.u.)	$\kappa(\omega)$ (Å^{-1})
0.20	0	0.133(8)	0.049(13)
0.20	0.005	0.111(6)	0.156(13)
0.25	0	0.123(8)	0.087(19)
0.25	0.01	0.111(5)	0.160(19)

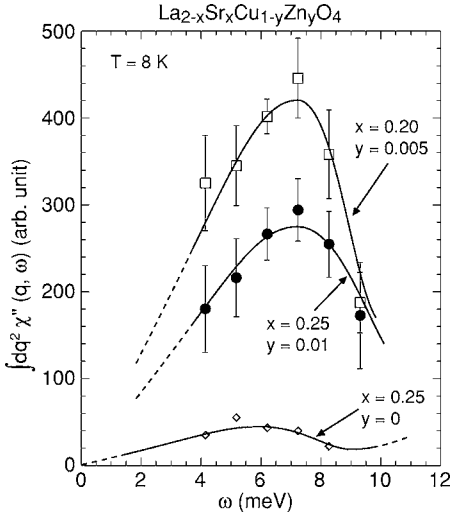

FIG. 7. ω-dependence of q-integrated dynamic spin susceptibility of LSCZO samples together with the data for the Zn-free LSCO with $x=0.25$ referred from Ref. 27. The lines are guides to the eye.

dynamic spin susceptibility $\int dq^2\chi''(\mathbf{q},\omega)$ where the integration is carried out over the four rods. Corresponding to the enhancement shown in Figs. 5 and 6, the Zn-substituted samples have a large integrated χ''. The Zn-free overdoped samples have been reported to have no clear spin gap down to $\omega=2$ meV and show a linear increase with ω.[27] For the Zn-doped samples, no spin gap is observed down to $\omega=4$ meV and, moreover, no static magnetic peaks are observed. At $\omega\leqslant 4$ meV, we presume a linear dependence with ω similar to that of the Zn-free samples as illustrated in Fig. 7. Notably, the spectra for the samples doped with Zn retain their maxima at $\omega\sim 7$ meV which is very close to the energy where χ'' of the Zn-free overdoped samples have their maxima.[27] This is in contrast to the case of Zn-substituted optimally doped LSCO $x=0.15$.[39,40] In this case, while the χ'' spectrum of Zn-free $x=0.15$ has a gap below ~ 4 meV and a maximum at $\omega=8$ meV, Zn substitution gives rise to significant spectral weight inside the gap and with further substitution static ($\omega=0$) spin-density-wave (SDW) order appears. This difference is discussed in detail in the next section.

V. DISCUSSION

Our measurements of the uniform magnetic susceptibility, that is $q=0$ measurements, have revealed that a paramagnetic moment is induced by both Zn substitution and by Sr overdoping for $x\geqslant 0.22$ and in both cases the superconductivity is perturbed in the same manner. On the other hand, the neutron scattering around $q=(\pi,\pi)$ demonstrates an anomalous enhancement of the dynamic AF correlations as a result of Zn substitution while the Zn-free sample shows a monotonic decrease in χ'' with increasing Sr concentration for $x\geqslant 0.25$.[27] In this section we discuss the observed phenomena in detail to reconcile these observations.

A. Paramagnetism and superconductivity

The suppression of T_c by magnetic perturbations has been discussed in pioneering work by Abrikosov and Gor'kov.[41] Oda *et al.*[29] found that the decrease of T_c as a function of the Curie constant C for both overdoped LSCO and LBCO without Zn follows the Abrikosov-Gor'kov (AG) theory. In the present study, because of our limited amount of data, fits of the data in Fig. 4 to the AG theory itself yields results with unacceptably large uncertainties. Hence we utilized a linear function which is a reasonable approximation when the magnetic impurity concentration is small. The agreement of the slope α for both the Zn-substituted and Sr-overdoped systems shown in Fig. 4 provides the important insight that the T_c suppression with increasing Sr concentration in the overdoped region of LSCO is concomitant with the induced paramagnetic moments as in the case of Zn substitution.

The Curie constant is related to the local moment by

$$C=\frac{Np_{eff}^2\mu_B^2}{3k_B}, \tag{7}$$

where N is the number of induced paramagnetic spins and p_{eff} is the effective moment in units of μ_B. Using this formula with the assumption that $N=N_{\mathrm{Zn}}$ (N_{Zn} is the number of Zn impurities), for the Zn-substituted samples of the present study one finds $p_{eff}=1.2(\pm 0.3)/\mathrm{Zn}$. This is in agreement with the previous result of $p_{eff}=1/\mathrm{Zn}$ for the Sr-underdoped regime of $0.05\leqslant x\leqslant 0.15$.[42] This is consistent with the intuitive picture that a nonmagnetic impurity breaks up a local AF pair thence yielding a single free spin. Perhaps more surprisingly, Sr-overdoped samples without Zn give $p_{eff}=0.5(\pm 0.1)/\mathrm{Sr}$ if we assume $N=N_x-N_{0.22}$, that is, based on the empirical results, p_{eff} is assumed to be given by the concentration of Sr ions that exceed $x=0.22$. An alternative approach is to assume that the induced moment $p_{eff}=\sqrt{g^2S(S+1)}$ with $S=1/2$ is always 1. In this case, the change of p_{eff} in the Sr case would be absorbed by a change in the number of local moments N given by $N=(N_x-N_{0.22})/4$. This implies that $\sim 1/4$ of the Sr ions that exceed $x=0.22$ induce pair-breaking of the local AF pairs.

It is an open question how 1/4 of the overdoped Sr or holes create the paramagnetic moment. As a possible scenario, 1/4 of the overdoped Sr^{2+} ions could substitute on the Cu sites instead of the La sites and thus act as nonmagnetic impurities. Since the LSCO system tends to be oxygen-vacant in the overdoped regime, this might be crystallographically possible even though Sr^{2+} has a larger ionic radius than Cu^{2+}. However, in our view this is not likely since the effects on the dynamic AF correlation are fundamentally different between Zn substitution and Sr overdoping as we will discuss later. Alternatively, an origin based on the overdoped holes, rather than the doped ions themselves, may be possible; for example, if 1/4 of overdoped holes were to choose the Cu $3d$ orbital rather than O $2p$, this would result in the elimination of the Cu local moment just as in the case of Zn substitution. Further study is necessary to obtain a microscopic understanding.

B. Zn-impurity effects on AF correlations

Based on their μSR measurements, Nachumi *et al.*[32] have suggested a "swiss-cheese" model of the Zn impurity effects. In this model, the magnetically affected area is located

around the impurity Zn ion and, therefore, the observed enhancement of the spectral weight in χ'' must originate from this area. As shown in Table II, $\kappa(\omega)$ for the Zn-substituted samples exhibits the same value ~ 0.16 Å^{-1} in spite of the different $\kappa(\omega)$ values of the Zn-free samples. Correspondingly, the affected area has a length scale of $1/\kappa(\omega) \simeq 6$ Å in the overdoped case which is quite a bit smaller than in the case of the optimally and underdoped LSCO.

As shown in Fig. 7, χ'', which is greatly enhanced by a small amount of Zn substitution, nevertheless still peaks at $\omega = 7$ meV. This is qualitatively different from the behavior in the optimally doped LSCO case. As revealed by neutron scattering, a small amount of Zn impurity ($y \leqslant 0.01$) in optimally doped LSCO induces spectral weight in χ'' in the spin-gap energy region and, furthermore, spin-density-wave order develops with further Zn substitution ($y = 0.017$).[39,40] Our results for the *overdoped* LSCO with Zn do not show either detectable SDW order or a spectral peak shift to lower energies in comparison to the Zn-free samples. We speculate that the overdoped sample has a characteristic spin fluctuation frequency that is higher than that in the optimally doped sample and therefore the induced χ'' peaks at a higher ω in the overdoped case than in the optimal case. This may also be the reason why no static SDW state develops in overdoped LSCO substituted with Zn as shown by the absence of a wipeout effect observed by nuclear quadrupole resonance[43] and the absence of static magnetic order observed by muon-spin-relaxation (μSR).[44]

Another important insight into the nature of the overdoped cuprates has been suggested by μSR; the muon-spin-relaxation rate σ which is proportional to the SC carrier density decreases with increasing doping in overdoped $Tl_2Ba_2CuO_{6+\delta}$.[45,46] This has been attributed to microscopic phase separation of the charge carriers into local Cooper-paired SC states and unpaired Fermi liquid (FL) states. The decreasing T_c in the overdoped region is correlated with a corresponding decrease in the SC volume fraction.[33] This scenario can be reconciled with our neutron scattering observations if we assume that the SC regions retain dynamic AF spin correlations that support Cooper pair formation while the FL region has no AF correlations and concomitantly no superconductivity.

In this scenario, the linear decrease of χ'' with T_c observed in Ref. 27 can be naturally understood as originating from the decrease of the SC volume fraction. The complete disappearance of χ'' in the nonsuperconducting $x = 0.30$ sample signifies the 100% volume fraction of the FL region. The microscopic phase separation scenario also predicts a critical threshold of the hole concentration for the phase separation, implying a constant hole concentration in the SC regions in the overdoped samples. Our observations exhibit related effects on the AF correlations by Zn impurities in both the $x = 0.20$ and 0.25 samples. Specifically, the induced magnetic peaks have the same $\kappa(\omega)$ and δ, and furthermore, the induced χ'' has a maximum at the same energy, $\omega = 7$ meV, in both samples. The only difference is that the enhancement of χ'' is smaller for $x = 0.25$ than for $x = 0.20$. Since the induced AF correlations originate from the SC region, the constancy of $\kappa(\omega)$ and δ is consistent with the constant hole concentration in the SC regions. Furthermore, the smaller enhancement of χ'' in the $x = 0.25$ sample compared with that in the $x = 0.20$ sample can be attributed to the smaller SC volume fraction in the $x = 0.25$ sample. Consistent with this, our preliminary measurement shows that Zn substitution into a $x = 0.30$ sample which has no SC fraction shows no evidence for the inducement of observable AF correlations.

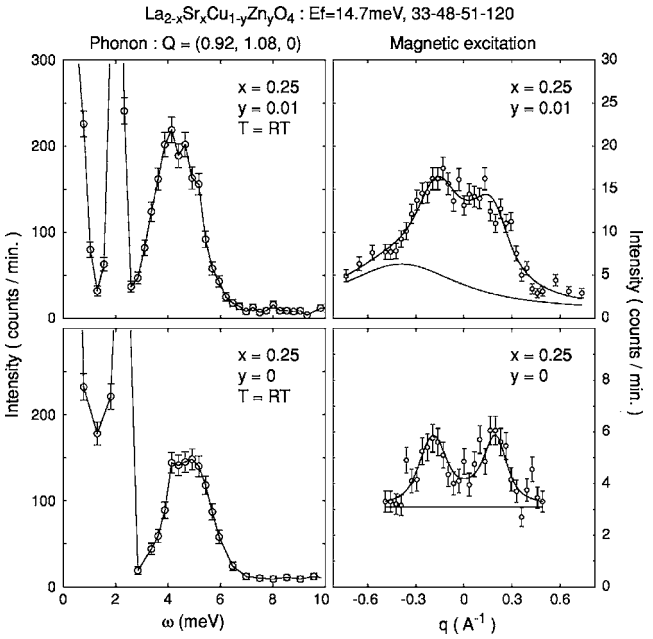

FIG. 8. Raw data of phonon (left) and magnetic peaks (right) for the $x = 0.25$ samples without and with Zn. All profiles are measured at the C5 spectrometer with fixed $E_f = 14.5$ meV and a collimation sequence of 33′-48′-51′-120′. The magnetic cross sections are collected by counting for 10 min/point for the Zn-doped and 20 min/point for the Zn-free samples.

VI. CONCLUDING REMARKS

We have measured the uniform magnetic susceptibility and neutron scattering of overdoped LSCO with and without Zn impurities. Uniform susceptibility measurements show clearly that the superconductivity in the overdoped region is perturbed by the induced Curie paramagnetism. On the other hand, our neutron scattering results are consistent with a microscopic phase separation scenario into local superconducting and Fermi liquid regions. To reconcile these facts, it is natural to speculate that the paramagnetic Curie behavior originates from the nonsuperconducting Fermi liquid region in the Zn-free samples. It is important to elucidate microscopically how the overdoped Sr ions or associated holes create the paramagnetic moments and the Fermi-liquid regions simultaneously.

As for the Zn-doped LSCO for $x \geqslant 0.20$, we have observed a surprisingly large enhancement of the AF correlations around $(\pi\ \pi)$ by a tiny amount of Zn impurity. The enhancement in the overdoped samples far exceeds that in the optimally doped LSCO.[39,40] As we discussed, our observations appear to be qualitatively consistent with the swiss-

cheese model that limits the Zn impurity effect on the magnetism to the area around the Zn ions. It is, however, disputable quantitatively that a small area around the Zn-impurities causes such a huge effect. To elucidate the origin of the enhancement, it is also important to study the Zn effects on the spin excitations in the high energy region.

Finally, our measurements have evinced remarkable changes in the magnetic properties from the optimally doped to the overdoped regime: appearance of the Curie paramagnetism and anomalous enhancement of AF correlations by Zn impurities. Moreover, around the lower boundary of the overdoped region, the conductivity changes from unusual-metallic to normal-metallic behavior; other measurements suggest that the pseudogap closes in this same crossover region. These facts may imply an intriguing phase crossover between the optimally doped and overdoped regions around $x=0.20$ which is crucial to the superconductivity. Further theoretical and experimental studies of this crossover should give new insights into the physics of high-T_c superconductivity.

ACKNOWLEDGMENTS

The authors thank Z. Tun, J. M. Tranquada, C. Stock, G. Shirane, M. Matsuda, B. Khaykovich, K. Kakurai, Y. Endoh, and W. J. L. Buyers for invaluable discussions. Work at the University of Toronto is part of the Canadian Institute of Advanced Research and supported by the Natural Science and Engineering Research Council of Canada, while research at Tohoku University is supported by a Grant-in-Aid from the Japanese Ministry of Education, Culture, Sports, Science and Technology.

APPENDIX

To compare the magnetic profiles of the different samples directly, the normalization has been made based on phonon intensities using Eqs. (4) and (5). The left-side figures in Fig. 8 show raw data of phonon peaks of the $x=0.25$ samples with and without Zn measured at $\mathbf{Q}=(0.92,1.08,0)$, using the same spectrometer configuration. The peak at ~ 2 meV adjacent to the phonon peak at ~ 4.5 meV originates from the tail of the nuclear Bragg peak detected by the edge of the resolution ellipsoid, proving that scans are made on the focusing side. Since the data are taken by fixing the final energy E_f, first the data have been corrected for higher order neutrons monitor rates at each incident energy E_i. Those for the Chalk River Reactor have been measured and reported in Ref. 17, while those for the JAERI reactor have been determined by a general formula in Ref. 47. Then the phonon peaks have been fitted by a Gaussian line shape to evaluate the phonon integrated intensity I in Eq. (5). Thus one can now evaluate the parameter A.

Using the A obtained above in Eq. (4), the observed magnetic cross section may be directly connected to $\chi''(\mathbf{Q},\omega)$ as normalized. For this purpose, we estimated the net magnetic intensity by subtracting the background. The figures on the right in Fig. 8 show the observed raw profiles of the magnetic peaks. While the figures are shown as the intensity for 1 min counting time, the actual measurements were done by counting for 10 min for the Zn-doped sample and for 20 min for the Zn-free sample. In analyses of the most corrected profiles, we have used a flat or sloping background. For the profile of the Zn-doped $x=0.25$ sample shown in the right-top figure, however, we have utilized a broadly peaked background since the wide-ranged profile naturally implies such a background. Unfortunately, we were not able to determine the origin of the peaked background; however, assuming either a sloped or peaked background does not affect the results dramatically. The background-subtracted magnetic intensities have been corrected for higher order neutron monitor rates and then the obtained cross section has been determined as $\partial^2\sigma/\partial\Omega\partial\omega$ in Eq. (4). Finally, the normalized $\chi''(\mathbf{Q},\omega)$ shown in Fig. 5 are obtained from the raw data shown in Fig. 8.

*Corresponding author. Email address: swakimoto@neutrons.tokai.jaeri.go.jp

[1] H. Yoshizawa, S. Mitsuda, H. Kitazawa, and K. Katsumata, J. Phys. Soc. Jpn. **57**, 3686 (1988).
[2] R. J. Birgeneau, Y. Endoh, K. Kakurai, Y. Hidaka, T. Murakami, M. A. Kastner, T. R. Thurston, G. Shirane, and K. Yamada, Phys. Rev. B **39**, 2868 (1989).
[3] S.-W. Cheong, G. Aeppli, T. E. Mason, H. Mook, S. M. Hayden, P. C. Canfield, Z. Fisk, K. N. Clausen, and J. L. Martinez, Phys. Rev. Lett. **67**, 1791 (1991).
[4] K. Yamada, C. H. Lee, K. Kurahashi, J. Wada, S. Wakimoto, S. Ueki, H. Kimura, Y. Endoh, S. Hosoya, G. Shirane, R. J. Birgeneau, M. Greven, M. A. Kastner, and Y. J. Kim, Phys. Rev. B **57**, 6165 (1998).
[5] S. Wakimoto, G. Shirane, Y. Endoh, K. Hirota, S. Ueki, K. Yamada, R. J. Birgeneau, M. A. Kastner, Y. S. Lee, P. M. Gehring, and S. H. Lee, Phys. Rev. B **60**, R769 (1999).
[6] S. Wakimoto, R. J. Birgeneau, M. A. Kastner, Y. S. Lee, R. Erwin, P. M. Gehring, S. H. Lee, M. Fujita, K. Yamada, Y. Endoh, K. Hirota, and G. Shirane, Phys. Rev. B **61**, 3699 (2000).
[7] M. Matsuda, M. Fujita, K. Yamada, R. J. Birgeneau, M. A. Kastner, H. Hiraka, Y. Endoh, S. Wakimoto, and G. Shirane, Phys. Rev. B **62**, 9148 (2000).
[8] M. Fujita, K. Yamada, H. Hiraka, P. M. Gehring, S.-H. Lee, S. Wakimoto, and G. Shirane, Phys. Rev. B **65**, 064505 (2002).
[9] K. Machida, Physica C **158**, 192 (1989).
[10] H. J. Schulz, J. Phys. (France) **50**, 2833 (1989).
[11] J. Zaanen and O. Gunnarsson, Phys. Rev. B **40**, R7391 (1989).
[12] V. J. Emery, S. A. Kivelson, and O. Zachar, Phys. Rev. B **56**, 6120 (1997).
[13] P. Dai, H. A. Mook, and F. Dogan, Phys. Rev. Lett. **80**, 1738 (1998).
[14] H. A. Mook, P. Dai, S. M. Hayden, G. Aeppli, T. G. Perring, and F. Dogan, Nature (London) **395**, 580 (1998).

[15] M. Arai, T. Nishijima, Y. Endoh, T. Egami, S. Tajima, K. Tomimoto, Y. Shiohara, M. Takahashi, A. Garrett, and S. M. Bennington, Phys. Rev. Lett. **83**, 608 (1999).
[16] P. Dai, H. A. Mook, R. D. Hunt, and F. Dogan, Phys. Rev. B **63**, 054525 (2001).
[17] C. Stock, W. J. L. Buyers, R. Liang, D. Peets, Z. Tun, D. Bonn, W. N. Hardy, and R. J. Birgeneau, Phys. Rev. B **69**, 014502 (2004).
[18] L. P. Regnault, P. Bourges, P. Burlet, J. Y. Henry, J. Rossa-Mignod, Y. Sidis, and C. Vettier, Physica B **213&214**, 48 (1995).
[19] H. F. Fong, P. Bourges, Y. Sidis, L. P. Regnault, J. Bossy, A. Ivanov, D. L. Milius, I. A. Aksay, and B. Keimer, Phys. Rev. B **61**, 14773 (2000).
[20] H. F. Fong, P. Bourges, Y. Sidis, L. P. Legnault, A. Ivanov, G. D. Gu, N. Koshizuka, and B. Keimer, Nature (London) **398**, 588 (1999).
[21] H. He, P. Bourges, Y. Sidis, C. Ulrich, L. P. Regnault, S. Pailhes, N. S. Berzigiarova, N. N. Kolsenikov, and B. Keimer, Science **295**, 1045 (2002).
[22] S. M. Hayden, H. A. Mook, P. Dai, T. G. Perring, and F. Dogan, Nature (London) **429**, 531 (2004).
[23] C. Stock, W. J. L. Buyers, R. A. Cowley, P. S. Clegg, R. Coldea, C. D. Frost, R. Liang, D. Peets, D. Bonn, W. N. Hardy, and R. J. Birgeneau, Phys. Rev. B **71**, 024522 (2005).
[24] D. Reznik, P. Bourges, L. Pintschovius, Y. Endoh, Y. Sidis, T. Masui, and S. Tajima, Phys. Rev. Lett. **93**, 207003 (2004).
[25] J. M. Tranquada, H. Woo, T. G. Perring, H. Goka, G. D. Gu, G. Xu, M. Fujita, and K. Yamada, Nature (London) **429**, 534 (2004).
[26] N. B. Christensen, D. F. McMorrow, H. M. Ronnow, B. Lake, S. M. Hayden, G. Aeppli, T. G. Perring, M. Mangkorntong, M. Nohara, and H. Tagaki, Phys. Rev. Lett. **93**, 147002 (2004).
[27] S. Wakimoto, H. Zhang, K. Yamada, I. Swainson, Hyunkyung Kim, and R. J. Birgeneau, Phys. Rev. Lett. **92**, 217004 (2004).
[28] D. C. Johnston, Phys. Rev. Lett. **62**, 957 (1989).
[29] M. Oda, T. Nakano, Y. Kamada, and M. Ido, Physica C **183**, 234 (1991).
[30] T. Nakano, M. Oda, C. Manabe, N. Momono, Y. Miura, and M. Ido, Phys. Rev. B **49**, 16000 (1994).
[31] T. Nakano, N. Momono, T. Nagata, M. Oda, and M. Ido, Phys. Rev. B **58**, 5831 (1998).
[32] B. Nachumi, A. Keren, K. Kojima, M. Larkin, G. M. Luke, J. Merrin, O. Tchernyshöv, Y. J. Uemura, N. Ichikawa, M. Goto, and S. Uchida, Phys. Rev. Lett. **77**, 5421 (1996).
[33] Y. J. Uemura, Solid State Commun. **126**, 23 (2003).
[34] S. Hosoya, C. H. Lee, S. Wakimoto, K. Yamada, and Y. Endoh, Physica C **235–240**, 547 (1994).
[35] C. H. Lee, N. Kaneko, S. Hosoya, K. Kurahashi, S. Wakimoto, K. Yamada, and Y. Endoh, Semicond. Sci. Technol. **11**, 981 (1998).
[36] H. Takagi, R. J. Cava, M. Marezio, B. Batlogg, J. J. Krajewski, W. F. Peck, Jr., P. Bordet, and D. E. Cox, Phys. Rev. Lett. **68**, 3777 (1992).
[37] C. H. Lee, K. Yamada, Y. Endoh, G. Shirane, R. J. Birgeneau, M. A. Kastner, M. Greven, and Y.-J. Kim, J. Phys. Soc. Jpn. **69**, 1170 (2000).
[38] C. H. Lee, K. Yamada, H. Hiraka, C. R. Venkateswara Rao, and Y. Endoh, Phys. Rev. B **67**, 134521 (2003).
[39] H. Kimura, M. Kofu, Y. Matsumoto, and K. Hirota, Phys. Rev. Lett. **91**, 067002 (2003).
[40] M. Kofu, H. Kimura, and K. Hirota, Phys. Rev. B **72**, 064502 (2005).
[41] A. A. Abrikosov and L. P. Gor'kov, Sov. Phys. JETP **12**, 1243 (1961); M. Tinkham, *Introduction to Superconductivity* (McGraw-Hill, New York, 1996).
[42] G. Xiao, M. Z. Cieplak, and C. L. Chien, Phys. Rev. B **42**, 240 (1990).
[43] H. Yamagata, H. Miyamoto, K. Nakamura, M. Matsumura, and Y. Itoh, J. Phys. Soc. Jpn. **72**, 1768 (2003).
[44] C. Panagopoulos, A. P. Petrovic, A. D. Hillier, J. L. Tallon, C. A. Scott, and B. D. Rainford, Phys. Rev. B **69**, 144510 (2004).
[45] Y. J. Uemura, A. Karen, L. P. Le, G. M. Luke, W. D. Wu, Y. Kubo, T. Manako, Y. Shimakawa, M. Subramanian, J. L. Cobb, and J. T. Market, Nature (London) **365**, 805 (1993).
[46] Ch. Niedermayer, C. Bernhard, U. Binninger, H. Glückler, J. L. Tallon, E. J. Ansaldo, and J. I. Budnick, Phys. Rev. Lett. **71**, 1764 (1993).
[47] G. Shirane, S. M. Shapiro, and J. M. Tranquada, *Neutron Scattering with a Triple Axis Spectrometer* (Cambridge University Press, Cambridge, England, 2002).